JOURNAL OF IMAGING SCIENCE AND TECHNOLOGY® • Volume 47, Number 5, September/October 2003

A Model of Electrophotographic Laser Printing that is Independent of Halftone Algorithm

J. S. Arney,▲ P. G. Anderson▲ and Sunadi Gunawan

Center for Imaging Science, Rochester Institute of Technology, Rochester, New York, USA

A printer model for an electrophotographic printer is described that is capable of showing quantitatively the difference in behavior of different halftone patterns. The objective was to develop a model that is independent of the halftone pattern but as computationally simple as possible. A model employing a single point spread function was not found to be sufficiently reliable for this purpose. The model that was finally tested incorporated a point spread function for the distribution of toner mass, a toner delivery function, and a separate point spread function for scattering of light within the paper. The result was found to provide an accurate model of an electrophotographic printer that modeled the printing process quite well for a wide range of halftone patterns with a wide range of spatial frequency characteristics.

Journal of Imaging Science and Technology 47: 455-462 (2003)

Introduction

As part of a project to explore optimum halftone algorithms for different printing technologies, we have begun to explore the feasibility of employing printer simulation models to evaluate and compare the performance of different halftone patterns. An appropriate printer model for this purpose would allow different halftone patterns to be tested and evaluated rapidly without the need to print and measure actual samples. Such a model would have to be capable of simulating the printer process accurately with a minimum of calibration against the actual printer, and the model would have to be independent of the halftone algorithm used in the calibration process. In the current report, we describe a monochrome printer model developed for electrophotographic laser printing that appears to have these capabilities.

Approach for Developing a Laser Electrophotographic Printer (EP) Model

A successful, halftone-independent printer model must account for a phenomenon called dot gain, which is the difference in the nominal gray level sent to the printing device and the actual reflectance that is printed.[1,2] The dot gain phenomenon is typically divided into two phenomenological categories: physical dot gain and optical dot gain. The latter is an optical phenomenon involving lateral scattering of light in the paper substrate and can be rigorously described by an optical point spread function, PSF, or its Fourier equivalent, the paper MTF.[3-6] Physical dot gain involves the physical spreading of toner in the printing process and might also be characterized by a PSF. A very simple printer model might be constructed with a single, overall printer PSF (or printer MTF) that includes the effects of both optical and physical dot gain.[7-9] However, our experience is that such an approach to printer modeling does not accurately predict tone reproduction for a wide range of halftone algorithms. This is not surprising since the relationship between the amount of toner in the image (C = grams/m^2) and the amount of light reflected by the image (R) are non-linearly related. In other words, the PSF of physical dot gain and the PSF of optical dot gain are not linearly related and are not well approximated by a single printer PSF.

The next level of complexity for a printer model involves a stepwise application of two PSF functions: one PSF for the spread of toner mass, and a second PSF for the scattering of light in the printed image. There is ample reason to suspect such a model might still be inadequate for comparing different halftone patterns since physical spreading of toner can occur as a result of many different processes in a printer. Toner mass distribution in an electrophotographic printer, for example, can be related to the laser beam profile, electrostatic edge effects on the photoconductor, characteristics of the development process, and spreading behavior during development and fixing. Nevertheless, the model described in this report employs only a single PSF to describe toner distribution.

Observational evidence illustrated in Fig. 1 suggests that a physical PSF function is not a sufficient descriptor of the printing process. Two halftone patterns were printed at the same nominal dot area fraction of F_n = 0.25. The toner dots in pattern (A) in Fig. 1 were defined to be the size of the addressability limit of the

Original manuscript received December 18, 2002

▲ IS&T Member

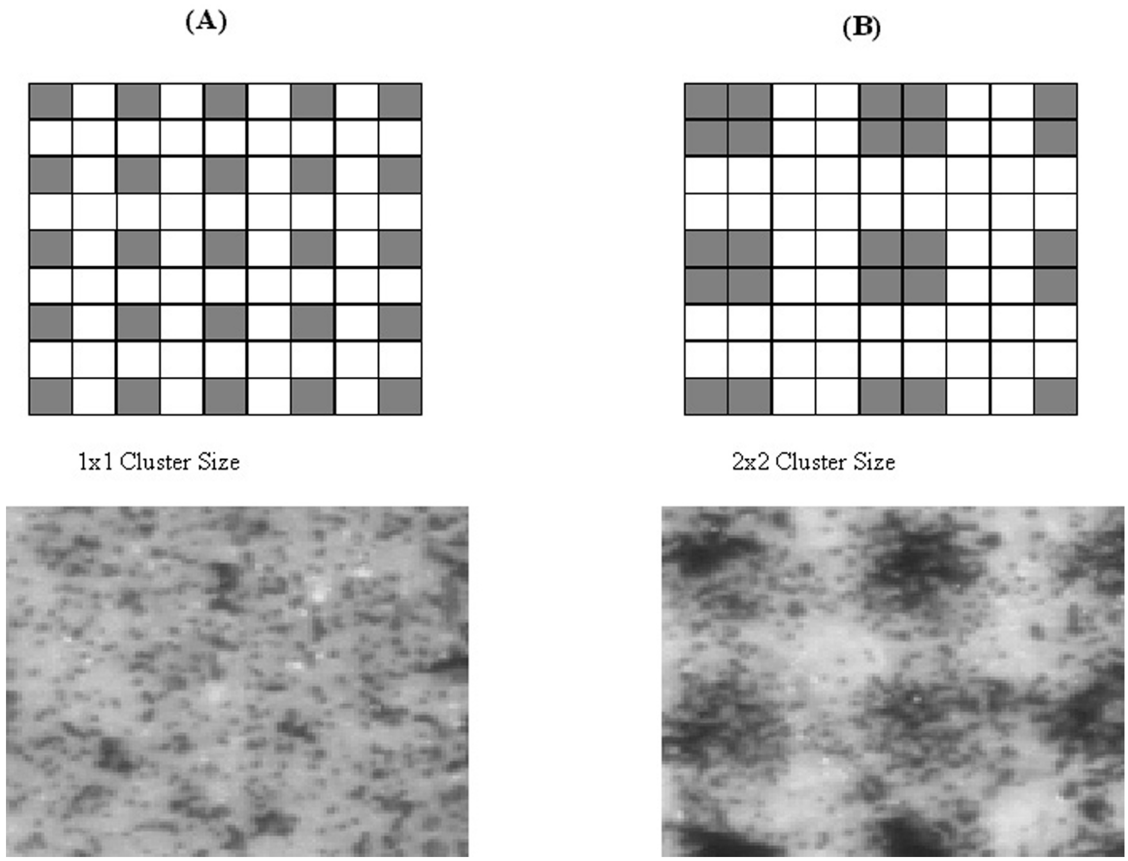

Figure 1. Image micrographs of samples printed at F_n = 0.25 with 1 × 1 and 2 × 2 cluster sizes.

printer. The printer used in this study was a 600 dpi HP Color Laserjet 4500, so the dots were defined at a size of 1/600th inch. The dots in pattern (B) were defined as 2 × 2 clusters of printer pixels for a size of 2/600th inch. Visual inspection of the samples strongly suggests the amount of toner per unit area delivered to a dot depends on the cluster size of the dot. Since a PSF is a type of probability density function, it is able to describe the way toner is distributed, but it can not account for an overall loss in the amount of toner that is delivered. This observation might suggest the need to model the printing process with more PSF functions, However, we have used an alternative approach. The model described in this project is a three-step model, illustrated in Fig. 2, involving the physical PSF to distribute toner, then a printer efficiency function to describe toner delivery to the final image, and finally the optical PSF of the paper.

The Printer Functions

The model begins with a pattern of 0 and 1 values defined by a halftone algorithm. This pattern is interpreted as an intended image of toner coverage, $C(x,y)$, where 0 means no toner and 1 means unity coverage of toner. Coverage, in mass/area, is in units relative to an image printed at a nominal dot area fraction of F_n = 1. The particular functions used to model the steps in Fig. 2 were selected arbitrarily to provide a reasonably good fit to experimental data, which will be described subsequently. The functions described below were found to provide a reasonably good model for the 600 dpi HP Color Laserjet 4500 used in this project.

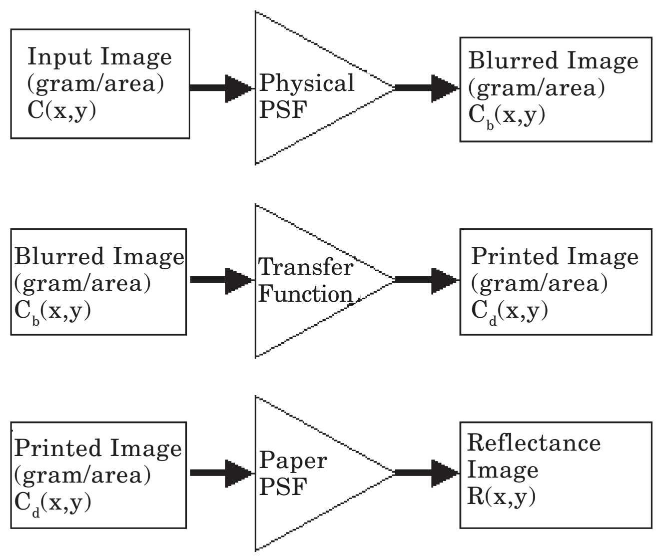

Figure 2. Stepwise Model of an Electrophotographic Printer

The first step of the model is to spread the input coverage, $C(x,y)$, by the physical PSF function. The function chosen to model the physical PSF is shown in Eq. 1. This function contains two parameters, p and σ, that will be adjusted to fit a calibration data set printed by the printer being modeled, and k is a normalization such that the integral of the PSF is unity. The value of σ models the width of the PSF and corresponds to the value of r where the PSF falls to half its maximum value.

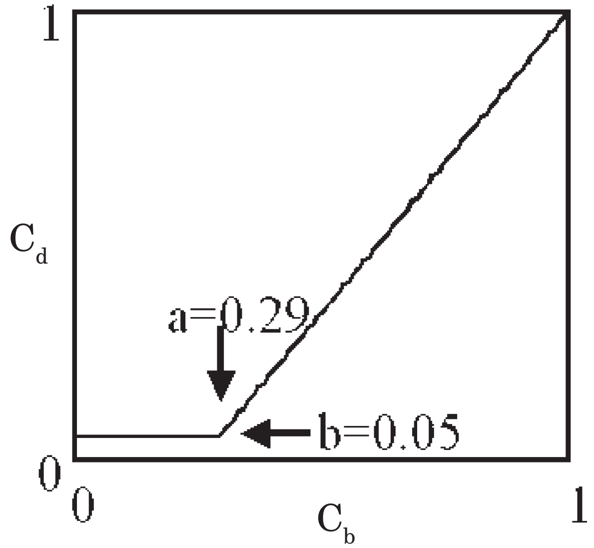

Figure 3. Toner transfer function

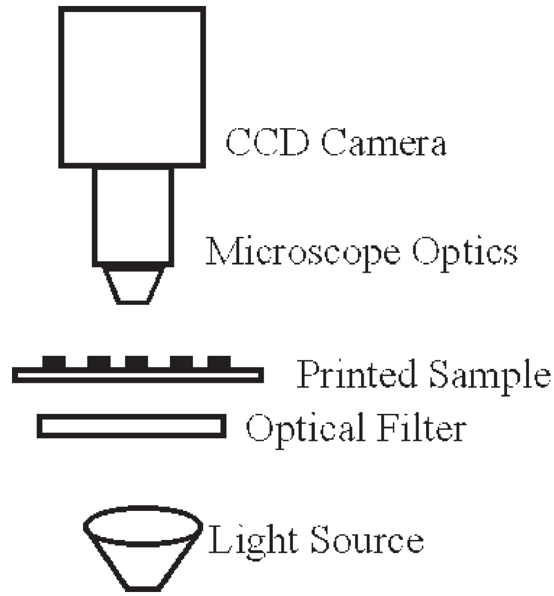

Figure 4. Schematic Illustration of microdensitometer used in transmission mode for toner coverage analysis.

The value of p governs the kurtosis of the PSF. Control of kurtosis was found, through trial and error, to fit experimental data better than a normal distribution with control only of σ. In order for the PSF to integrate to unity, the value of p is restricted to $p > 1$. This PSF function is convolved with the input coverage function, $C(x,y)$, to produce a blurred coverage function, $C_b(x,y) = C(x,y)*PSF(x,y)$.

$$\mathrm{PSF_P}(r) = \frac{k}{1+\left(\frac{r}{\sigma}\right)^p} \tag{1}$$

where

$$k = \frac{p \cdot \sin(\pi / p)}{\sigma \cdot \pi} \text{ and } r = \sqrt{x^2+y^2}\,.$$

The second step in the model applies the transfer function shown in Eq. (2) to the blurred toner distribution, $C_b(x,y)$. This is illustrated in Fig. 3. The result is the toner coverage that is delivered to the final image, C_d. The first two steps of the model constitute a model of the physical dot gain phenomenon.

$$C_d = (C_b - a)\left(\frac{1-b}{1-a}\right) \text{ for } C_b > a, \text{ else } C_d = b \tag{2}$$

The final step in the model describes the optical characteristics of the image. We begin by assuming the toner absorbs light but does not scatter light. This allows the use of Eq. (3), which converts toner coverage, $C_d(x,y)$, into a transmittance, $T(x,y)$. The constant in this equation, ε, is not a variable in the model. It is a constant determined experimentally by measuring the value of T for an experimentally printed sample at a dot area fraction of $F_n = 1$, where we define $C_d = 1$. The experimental method for measuring T will be described in detail below.

$$T(x,y) = \exp\{-\varepsilon \cdot C_d(x,y)\} \tag{3}$$

The transmittance distribution, $T(x,y)$ is converted to the final reflectance distribution of the image, $R(x,y)$, by applying the optical PSF_p of the paper as shown in Eq. (4), where R_g is the reflectance of the paper.

$$R(x,y) = R_g \cdot T(x,y) \cdot \left[\mathrm{PSF_P}(x,y) * T(x,y)\right] \tag{4}$$

Equation (4) is a well known function for optical dot gain, and the PSF_p function of paper has been thoroughly explored elsewhere.[4-6,9-11] The focus of the current project is on the first two steps of the model, Eqs. (1) and (2). A comparison between modeled values of $C_d(x,y)$ and experimental values of $C_d(x,y)$ can be made by adjusting the four model parameters, p, σ, a, and b. The experimental technique used to measure $C_d(x,y)$ is described below.

Optical Analysis of Toner Mass Distribution

A linear, calibrated CCD camera was mounted on a microscope in order to carry out microdensitometric measurements of the printed toner on paper. Measurements of the printed samples illuminated in reflection mode provided traditional measurements of tone reproduction, and measurements of this kind have been described previously.[12] However, reflection measurements of this kind can not be interpreted in terms of toner mass coverage on the paper. This is a consequence of the phenomenon of optical dot gain. Some of the light that passes through the dot into the paper will scatter laterally and reflect back to the camera from a region between the dots. Thus, some of the light measured between the dot carries the spectral signature of the toner. A quantitative absorption analysis based on reflection measurements will therefore misinterpret this light as an amount of toner between the dots even when no toner is actually present between the dots. In order to avoid this problem, the samples were illuminated in transmission mode as illustrated in Fig. 4.

Light captured in transmission mode is scattered as it passes through the paper. However, once it emerges

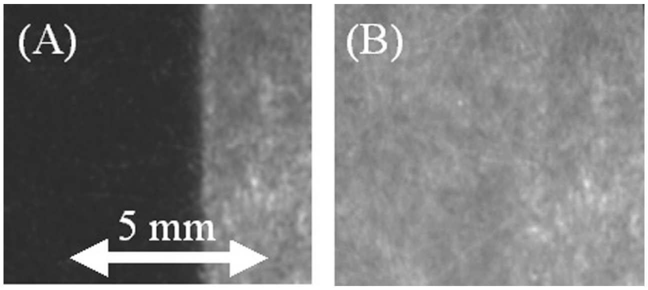

Figure 5. Edge between solid cyan and bare paper observed with (A) red light and (B) near infrared radiation.

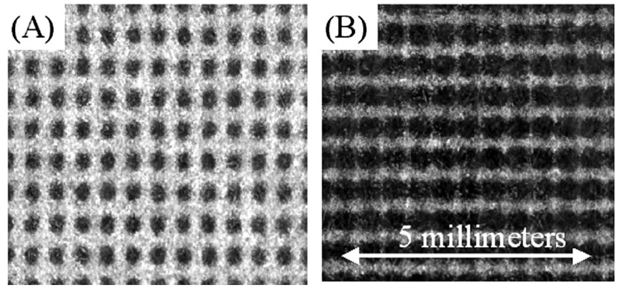

Figure 6. Transmittance images captured for cyan toner printed as clustered dot halftones at 100 LPI for (A) $F_n = 0.25$ and (B) $F_n = 0.56$.

from the paper it passes through the halftone dots once and does not return to the paper. Therefore, the light emerging from the dots carries the spectral signature of the toner, but light emerging between the dots does not, so there is no ambiguity about the spatial distribution of the toner. Equation 5 describes the distribution of image pixel values, $P(x,y)$, captured by the CCD camera as a function of the transmittance of the optical filter used in the instrument, the illumination distribution, I_o, the sensitivity distribution, S, of the camera/microscope system, the paper transmittance distribution, T_g , and the transmittance distribution of the toner, T.

$$P_r(x,y) = T_r \cdot I_o(x,y) \cdot S(x,y) \cdot T_g(x,y) \cdot T(x,y) \qquad (5)$$

The toner transmittance distribution, $T(x,y)$, is the object of the measurement. In order to extract this value from the measured image, $P(x,y)$, the other terms must be canceled. This was achieved for samples printed with cyan toner by capturing an image using a red filter, T_r, in the instrument, and then capturing a second image in registration with the first, but using an IR filter that blocks visible light and passed only near infrared light. The pixel values captured with the IR filter can be described with Eq. (6). As illustrated in Fig. 5, the toner does not absorb or scatter in the near infrared part of the spectrum. Thus, $T(x,y) = 1$ in Eq. (6).

$$P_{IR}(x,y) = T_{IR} \cdot I_{oIR}(x,y) \cdot S_{IR}(x,y) \cdot T_g(x,y) \cdot 1 \qquad (6)$$

Dividing Eq. (5) by Eq. (6) gives Eq. (7). Note that spatial variations associated with the paper and the instrument are canceled. We are left with terms $\bar{S}_r$ and $\bar{S}_{IR}$, which are the average sensitivity values of the CCD camera in the red and the near IR regions of the spectrum. In order to cancel these terms, we capture two reference images of a sample of paper with no toner printed on it. One is captured with

$$\frac{P(x,y)}{P_{IR}(x,y)} = \frac{T_r \cdot \bar{S}_r}{T_{IR} \cdot \bar{S}_{IR}} \cdot T(x,y) \qquad (7)$$

the red filter, $P_{ref}(x,y)$, and the other is captured with the IR filter, $P_{refIR}(x,y)$. These images are captured in registration, and their ratio cancels spatial variations of the paper and the instrument. Combining all four images produces Eq. (8), which is our experimental measure of the distribution of toner transmittance over the paper.

$$T(x,y) = \frac{P(x,y)\,P_{ref}(x,y)}{P_{IR}(x,y)\,P_{refIR}(x,y)} \qquad (8)$$

The average value of $T(x,y)$ for a sample printed at a nominal dot area fraction of $F_n = 1$ was measured and called T_1. Assuming Beer-Lambert optics for the cyan toner, we convert the measurements into a spatial map of the relative toner coverage with Eq. (9).

$$C(x,y) = \frac{\ln[T(x,y)]}{\ln[T_1]} \qquad (9)$$

Validation of the Analysis

In order to test the utility of the analytical procedure described above, cyan toner was printed on paper using the Laserjet 4500 printer. A conventional halftone mask was defined as a 6×6 array of pixels, each pixel representing one addressable unit of the 600 dpi printer. The halftone algorithm was a conventional clustered dot algorithm, so the printed images were 100 LPI halftones. Figure 6 illustrates images captured in transmitted light for samples printed at nominal dot area fractions $F_n = 0.25$ and $F_n = 0.56$. These images are useful for illustration, but quantitative analysis was based on the coverage map, $C(x,y)$, generated from the images with Eq. (9). The resulting coverage histograms for these images are shown in Fig. 7. Also shown are histograms for a plain, unprinted paper and for the solid cyan, $F_n = 1$.

These results show that the analysis suffers from some amount of experimental variance. This is seen in the spread of curve (C) in Fig. 7 for toner on plain paper. The coverage analysis shows some amount of negative coverage of toner on the paper. This is an experimental artifact and indicates the level of precision of the analysis, not the accuracy of the analysis. The primary cause of the spread in the peak of curve (C) can be attributed to a difference in focal length of the microscope lens between the red and the near IR. One image can be in good focus, but the other is slightly out of focus. This causes Eq. (8) to act somewhat like an unsharp mask algorithm. As a result, experimental variance from the formation pattern of the paper is substantially suppressed but not completely removed.

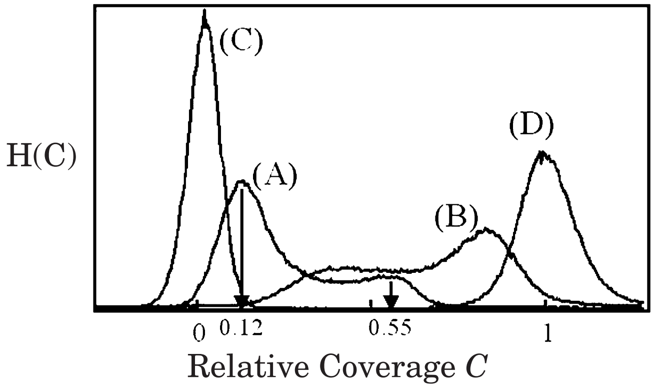

Figure 7. Coverage histograms for chan halftones. Samples (A) and (B) were printed at F_n = 0.25 and 0.55 and are illustrated in Fig. 6. Sample (C) is paper with no toner, and sample (D)is solid toner at F_n = 1.

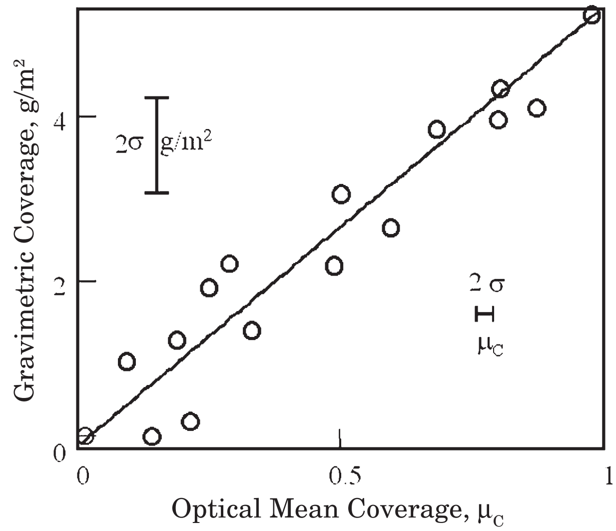

Figure 8. Comparison between gravimetric analysis of toner coverage in g/m² and optical mean relative coverage, μ_C. Error bars are mean values of 2σ for multiple measurements.

Figure 7 also shows that as the dot size increases, some toner is actually deposited on the paper between the dots. Curve (A), for example, shows that the paper between the halftone dots at F_n = 0.25 is not toner free. The average coverage of toner between the dots in (A) is C = 0.12, and the average coverage within the dots is C = 0.55. Treating the histogram function, $H(C)$ as a probability density function, the mean toner coverage, μ_C, on the printed image is obtained from Eq. (10).

$$\mu_C = \int_{-\infty}^{\infty} \mathrm{C} \cdot \mathrm{H(C)}\,\mathrm{dC} \tag{10}$$

The mean toner coverage can also be estimated by gravimetric analysis. Samples of single gray levels ranging from F_n = 0 to F_n = 1 were printed. Each gray level was printed so it covered the entire paper, and the printed paper samples were weighed. The mean weight of the same size paper printed with zero toner was subtracted, and the resulting mass of toner was divided by the area of the printed sample. The resulting coverage, in grams per meter², was plotted versus the relative mean coverage, μ_C, measured optically. Clearly the gravimetric analysis suffers from the intrinsic variability of paper, but the result indicates that the optical analysis can be used as an experimental estimator of toner coverage. Moreover, the regressed slope of the line in Fig. 8 provides a calibration for converting the results of the optical analysis from relative units to absolute units of grams/meter².

Calibration of the Printer Model

The printer model of Fig. 2 was constructed with four parameters, p, σ, a, and b, as described above. In order to estimate the values for these parameters that best represent the LaserJet 4500 used in this project, a set of clustered dot patterns at constant F_n was selected as a calibration set. These patterns are illustrated in Fig. 1 and included cluster sizes of 1 × 1, 2 × 2, 3 × 3, 4 × 4, 5 × 5, 7 × 7, and 9 × 9. Samples were printed with the Laserjet 4500 with cyan toner. Transmittance images were captured, as illustrated in Fig. 9, and relative coverage maps $C(x,y)$ were calculated.

The initial bi-level clustered dot patterns were run through the printer model to calculate a simulated coverage map, $C_{sim}(x,y)$, in relative coverage units. Comparison of the experimental coverage, $C(x,y)$, with the simulated coverage, $C_{sim}(x,y)$, was done by comparing the coverage histograms. From the histograms, values of mean coverage, μ_C, were calculated as described in Eq. (10), and values of RMS coverage deviation, σ_C, were calculated using Eq. (11). Calculations were done in relative coverage units.

$$\sigma_C = \sqrt{\int_{-\infty}^{\infty} (C - \mu_C)^2 \cdot \mathrm{H(C)}\,\mathrm{dC}} \tag{11}$$

The value of μ_C is a measure of the total amount of toner delivered in the printing process. For the test series with F_n = 0.25, the maximum possible value of μ_C is 0.25. A decrease in μ_C is a manifestation of a toner transfer curve, Fig. 3, that falls below a 1:1 straight line. A dot gain effect in which a spread phenomenon distributes toner without changing the total toner delivered would not change the value of μ_C.

The value of σ_C should depend both on the transfer curve and on the spread function. If the transfer curve is a 1:1 straight line, and if no spreading occurs, then σ_C is at the maximum possible value. It is easy to show that this maximum possible value of σ_C is given by Eq. (12). For the cluster patterns at F_n = 0.25, this maximum value is σ_{Cmax} = 0.433. Measured versus modeled values of μ_C and σ_C are shown in Fig. 10 for model parameters of σ = 37 μm, p = 5, a = 0.29, b = 0.05. These values produced the minimum average difference between the ideal slopes of 1.00 and ideal intercepts of 0.00.

$$\sigma_{\mathrm{Cmax}} = \sqrt{\mathrm{F_n} \cdot (1 - \mathrm{F_n})} \tag{12}$$

A visual comparison was also made between the printed and the modeled samples. Transmittance images were calculated for each modeled coverage map, and the results are shown in Fig. 11. Looking past the noise level in the experimental printed samples, the comparison between Figs. 9 and Fig. 11 appears quite reasonable.

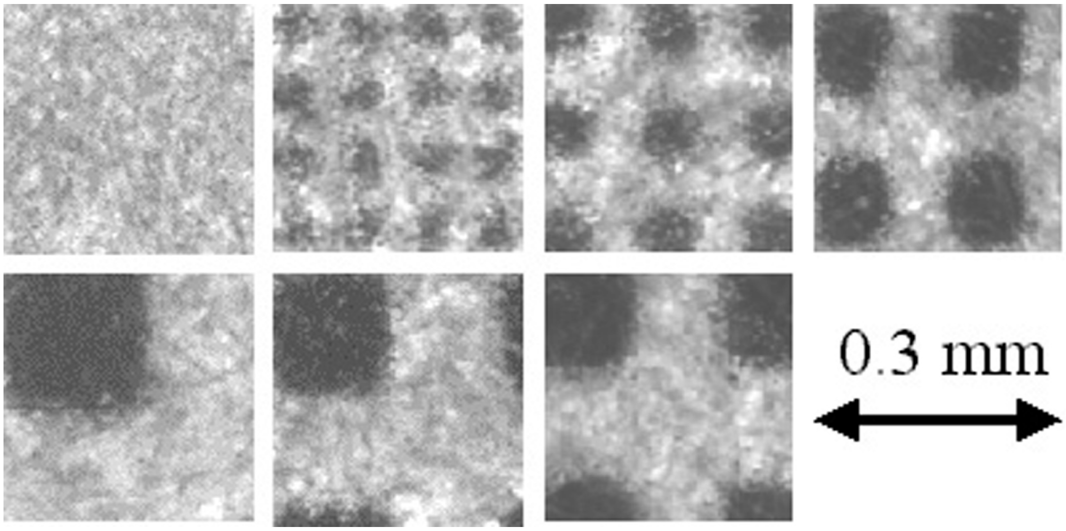

Figure 9. Calibration cluster patterns 1 × 1 through 9 × 9 printed and imaged in transmitted light.

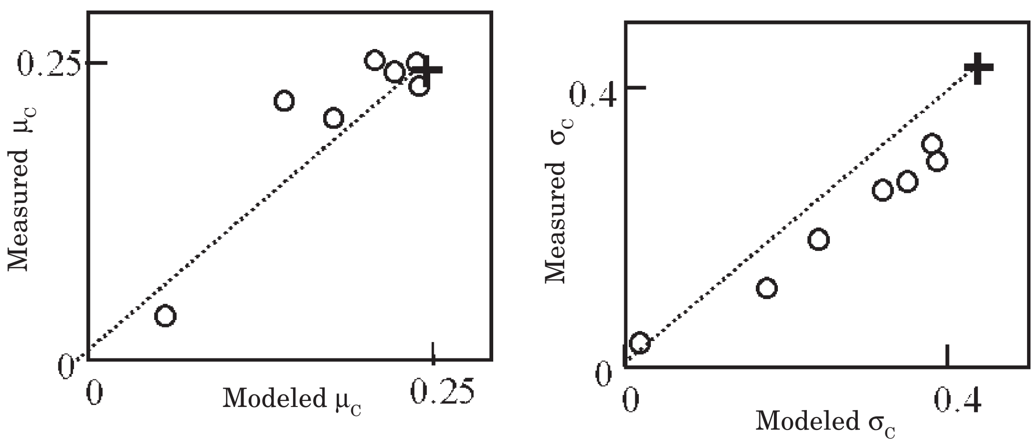

Figure 10. Measured versus modeled values of μ_C and σ_C for the cluster patterns at F_n = 0.25. Model parameters: σ_p = 37 µm, p = 5, a = 0.29, b = 0.05. The dotted line represents a perfect correlation, and + is the maximum possible value for Φ_v = 0.25.

Challenging the Printer Model

If this printer model is to be useful, it must be able to reproduce the behavior of the printer for a wide variety of halftone patterns without re-calibration. To test whether the model is capable of such performance, four halftone patterns representing a very wide range of spatial characteristics were printed with the Laserjet 4500 and with the virtual printer model. Each type of halftone pattern was printed at a series of nominal dot area fractions F_n from 0 through 1. At each gray level for each halftone pattern, printed samples were analyzed for their coverage maps, $C(x,y)$, and then for μ_C and σ_C. The corresponding values of μ_C and σ_C were calculated with the printer model using the four calibration values of σ_p = 37 mm, p = 5, a = 0.29, b = 0.05 determined from the calibration analysis described previously. The results are shown in Figs. 12 and 13. Note that the maximum theoretical values of μ_C and σ_C are 1.0 and 0.5 respectively.

The four halftone patterns in Figs. 12 and 13 were chosen to represent a very wide range of spatial frequency characteristics. Pattern (A) is a traditional Floyd-Steinberg pattern and represents a high frequency type of halftone. Pattern (D) is the lowest frequency pattern and is a clustered dot halftone at 100 lpi constructed from a 6 × 6 halftone mask. Patterns (B) and (C) were generated with an algorithm called linear pixel shuffling[13] and have noise power spectra with energy concentrated between the frequencies of (A) and (D). A Wiener spectrum analysis demonstrated that (C) has a broader frequency spectrum than (B).

The phenomenon called physical dot gain is represented in the model by the PSF_p function shown in Eq. (1). The effect of this function would be expected to be greatest on higher frequency halftones. Thus, the expectation is that both the measured and the modeled values of σ_C should decrease as we go from the low frequency halftone (D) to the Floyd-Steinberg (A). This effect is clearly displayed both by the experimentally printed samples and by the printer model.

Conclusion

It is certainly true that the printer model described in this work is a highly simplified representation of the actual processes that govern the spread and delivery of toner in an electrophotographic laser printer. Moreover, the experimental data shown in Figs. 12 and 13 show that the model does not perfectly reproduce the printing process. The upward sweep of the data in Fig. 12,

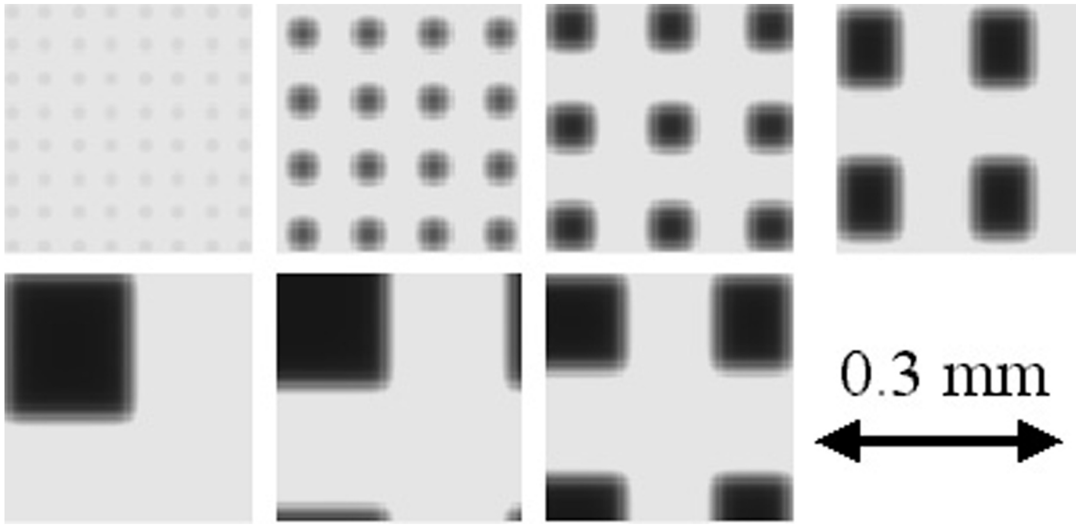

Figure 11. Cluster patterns 1×1 through 9×9 printed by the printer model. Compare with Fig. 9.

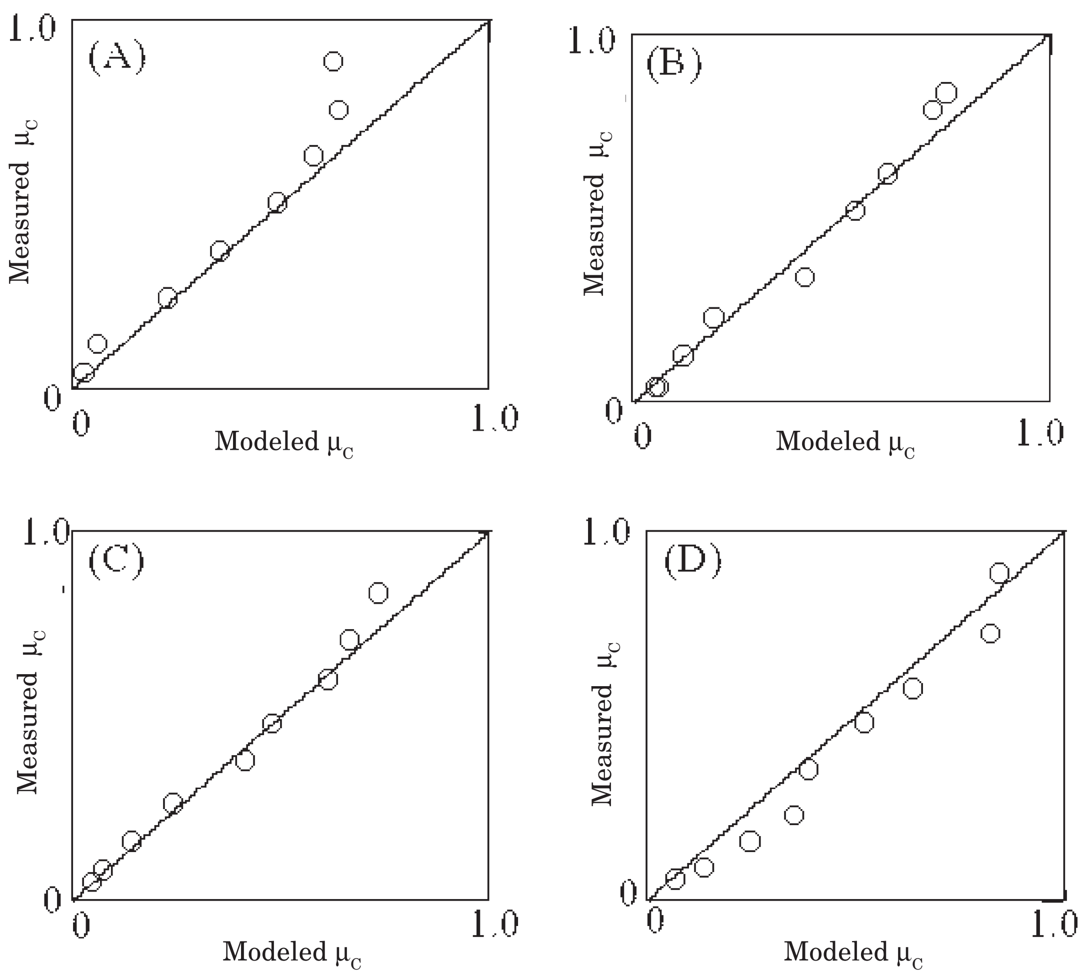

Figure 12. Measured versus modeled values of m_C for the four halftone gray ramps. (A) Floyd-Steinberg, (B)[13] LPS-1, (C) LPS-2, (D) Clustered dot at 100 LPI.

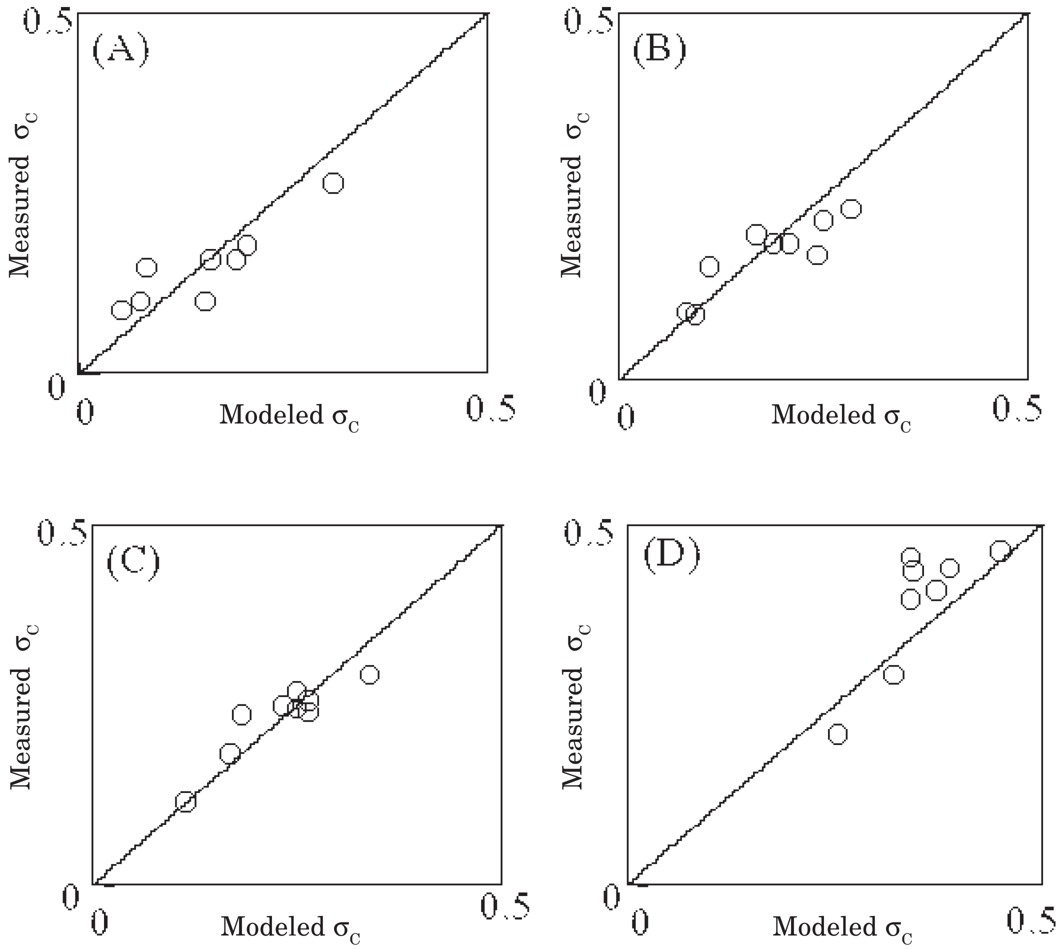

Figure 13. Measured versus modeled values of s_C for the four halftone gray ramps. (A) Floyd-Steinberg, (B)[13] LPS-1, (C) LPS-2, (D) Clustered dot at 100 LPI.

for example, and the low correlation coefficients in Fig. 13 may indicate inadequacies of the model. They also might indicate artifacts of the experimental analysis, and the authors are not yet sufficiently confident in the analytical procedure to distinguish between the two. Nevertheless, this approach to printer modeling appears to be a sufficiently accurate approximation of the printing process to justify further work on the development of improved analytical techniques and on the exploration of the model for searching for improved halftone patterns.

Expansion of this work into several additional projects is underway. First, variations of this model appropriate for other printing technologies is underway. Second, the authors plan to use this printer model as a foundation for construction of a noise propagation model, and thus expand the utility of the virtual printer. Finally, the authors are developing search and optimization algorithms that will incorporate printer models of this kind as a means of testing and optimizing a wide variety of halftone patterns. Results of these projects will be reported subsequently.

Acknowledgment. This project was sponsored by a grant from the Hewlet-Packard Corporation, with guidance from Norm Burningham and Ken Lindblom. Special thanks to Bob Chin, Manager of Digital Technologies in OMNOVA Solutions, Inc., for sponsorship of summer research support for undergraduate student participation in the project.

References

1. J. A. C. Yule and W. J. Neilsen, *TAGA Proc.*, 65 (1951).
2. J. A. C. Yule, D. J. Howe, and J. H. Altman, *TAPPI*, 337 (1967).
3. J.S. Arney, C. D. Arney, M. Katsube and P. G. Engeldrum, An MTF Analysis of Papers, *J. Imaging Sci. Technol*, **40**, 19 (1996).
4. P. Oittinen, *Advances in Printing Science and Technology*, vol. 16, W. H. Banks, Ed., Pentech Press, London, UK, 1982, pp. 121-128.
5. P. G. Engeldrum and B. Pridham, The Application of Turbid Medium Theory to Paper Spread Function Measurements, *TAGA Proc.*, 339 (1995).
6. G. L. Rogers, Optical Dot Gain: Lateral scattering Probabilities, *J. Imaging Sci. Technol*, **43**, 341 (1998).
7. S. Inoue, N. Tsumura and Y. Miyake, Measuring MTF of Paper by Sinusoidal Test Pattern Projection, *J. Imaging Sci. Technol.* **41**, 657(1997).
8. C. Koopipat, M. Fujino, K. Miyata, H. Haneishi, and Y. Miyake, Image Evaluation and Analysis of Ink Jet Printing System (I): MTF Measurement and Analysis of Ink Jet Image, *Proc. of IS&T PICS Conference*, IS&T, Springfield, VA, 2000, pp. 149-154.
9. C. Koopipat, N. Tsumura, Y. Miyake, and M. Fujino, Effect of Ink Spread and Opitcal Dot Gain on the MTF of Ink Jet Image, *J. Imaging Sci. Technol.* **46**, 321 (2002).
10. S. Gustavson, Modeling of Light Scattering Effects in Print, *J. Imaging Sci. Technol.* **41**, 283 (1997).
11. S. Mourad, K. Simon, P. Emmel, and R. D. Hersch, Extending Kubelka-Munk's Theory with Lateral Light Scattering, *Proc. IS&T's NIP17*, IS&T, Springfield, VA, 2001, p. 469.
12. J. S. Arney, C. Scigaj and P. Mehta, *J. Imaging Sci. Technol.* **45**, 466 (2001).
13. P. G. Anderson, J. Arney and K. Ayer, Linear Pixel Shuffling (I): New Paradigms, for New Printers, Proc. IS&T NIP16, IS&T, Springfield, VA, 2000.